Int. J. Heat Mass Transfer. Vol. 27, No. 7, pp. 1055–1065, 1984
Printed in Great Britain

0017–9310/84 $3.00 + 0.00

INWARD SOLID–LIQUID PHASE-CHANGE HEAT TRANSFER IN A RECTANGULAR CAVITY WITH CONDUCTING VERTICAL WALLS

C.-J. Ho* and R. Viskanta
School of Mechanical Engineering, Purdue University, West Lafayette, IN 47907, U.S.A.

(*Received* 7 *March* 1983 *and in revised form* 11 *October* 1983)

Abstract—This paper reports basic solid–liquid interface and heat transfer data obtained during solid–liquid phase change (melting and solidification) of n-octadecane in a two-dimensional rectangular cavity with conducting vertical walls. The shadowgraph technique was used to measure local heat transfer coefficients at the heat source surface. The solid–liquid interface motion during phase change was recorded photographically. During melting, a development of vortex motion at the bottom melt zone was observed to be quite similar to that in a rectangular cavity with isothermal walls. In both melting and solidification experiments the conducting walls acted as isothermal walls at the late times during the processes. Natural convection was found to control the melt shape, the melting rate and heat transfer during melting. The effect of the initial subcooling of the solid was also investigated and the results clearly showed that heat conduction was the dominant mode of energy transport during the inward solidification. For solid–liquid phase-change heat transfer short extended surfaces are more effective than longer ones.

NOMENCLATURE

AR	aspect ratio, H/W
c	specific heat
Fo	Fourier number, $\alpha t/W^2$
g	gravitational constant
H	height of cavity
Δh_f	latent heat-of-fusion
k	thermal conductivity
l_{eq}	equivalent length defined by equation (3)
Nu	local Nusselt number
$\overline{Nu}$	average Nusselt number, see equation (2)
Pr	Prandtl number
Ra	Rayleigh number
S_c	subcooling parameter, $c_s(T_f - T_i)/\Delta h_f$
S_h	superheating parameter, $c_l(T_i - T_f)/\Delta h_f$
Ste_l	Stefan number for melting, $c_l(T_w - T_f)/\Delta h_f$
Ste_s	Stefan number for solidification, $c_s(T_f - T_w)/\Delta h_f$
T	temperature
t	time
V	volume
X	coordinate measured horizontally from the left-vertical wall of the cavity
y	coordinate measured vertically from the bottom (base) of the cavity.

Greek symbol

τ	dimensionless time, $Fo\,Ste$.

Subscripts

b	bottom (base) of the cavity
h	heated surface
l	liquid
s	solid
w	wall
0	initial.

* Present address: Department of Mechanical Engineering, National Cheng-Kung University, Tainan, Taiwan.

INTRODUCTION

Solid–liquid phase-change heat transfer such as solidification and melting is not only of practical interest to a wide range of technologies but also in geophysics. The work described in this paper has been motivated by latent heat-of-fusion energy storage, but it may also have other applications. For example, in some latent heat-of-fusion energy storage concepts the phase-change material is encapsulated in containers or is placed on the shell side of a shell-and-tube heat exchanger [1]. The working fluid during charging and recovery cycles is circulated through flow passages in the unit. In the classical treatment of the phase-change problems convection in the liquid is neglected [2], and heat transfer is solely due to heat conduction. More recent experimental evidence has clearly established that both during solidification and melting, natural convection in the liquid can have an important or dominant influence on the motion and the shape of the phase-change boundary and on the rate of heat transfer [3].

Latent heat thermal energy storage devices exhibit certain self-defeating traits. The materials usually have low thermal conductivities and during the solidification or discharge process, the material solidifies onto the heat transfer surfaces, increases the thermal resistance, and acts as a self-insulator. One of the many possible ways of enhancing heat transfer in latent energy storage devices is the use of extended surfaces (fins) [1]. It was first suggested by Humphries [4] in connection with spacecraft thermal control. The thermal performance of finned storage units [5] and finned heat pipe storage modules has been investigated [6, 7]. The enhancement of solidification by finning has been studied experimentally for external arrangements [8, 9]. The effects of fins on heat conduction during solidification in two-dimensional (2-D) rectangular [10–12] and doubly connected [13, 14] geometries have also been examined analytically. Heinze and

Humphrey [11] presented a simplified numerical model for melting in a rectangular enclosure in which both the top and the bottom walls acted as fins. The model is based on a quasi-linear, transient thin-fin equation to predict the melting rate and the shape of the solid–liquid interface. A correlation for natural convection heat transfer coefficients was needed as an input to the model to account for the fluid motion in the melt. More recently, Smith and Koch [12] have obtained a numerical solution for a transient heat conduction problem with solidification occurring in a rectangular enclosure with conducting vertical sidewalls which act as one-dimensional (1-D) fins.

The present experimental study was undertaken to obtain solid–liquid phase-change (melting or solidification) heat transfer data in a 2-D rectangular enclosure formed by an isothermal bottom and two conducting vertical sidewalls. The bottom of the enclosure was subjected to an isothermal wall temperature boundary condition, while the top free surface was insulated. An air-gap between the material and the top of the enclosure was also maintained to accommodate for the volume change accompanying phase change in the material. Three different aspect ratio enclosures were used in the experiments. The results of the solid–liquid interface motion, interferometric visualization of the temperature distribution in the melt, and the local heat transfer at the heated bottom surface as well as along the conducting sidewalls during melting are presented. The experimental results for solidification are also discussed.

EXPERIMENTS

Test apparatus

The test apparatus consisted of a test cell, two constant temperature baths and data acquisition equipment. The local heat transfer measurements were made using a shadowgraph system, and a Mach–Zehnder interferometer was used for flow visualization.

The principal components of the test cell consisted of two aluminum vertical walls with a thickness of 4.8 mm, and a copper bottom plate with two Plexiglas windows. A schematic diagram showing the test cell is shown in Fig. 1. The inside dimensions were 40 mm deep, 48 mm wide, and different heights which depend on the aspect ratio of the enclosure desired. Three different heights of the aluminum wall, 25, 55, and 70 mm, were used in this study. This corresponds to aspect ratios of 0.42, 1.0, and 4.0, respectively. For an aspect ratio of 4, a smaller inner dimension of the test cell was used to reduce the length of time required for completing the phase-change experiments. In this case, the test cell was 15 mm wide, 70 mm high, and 40 mm deep.

The bottom surface of the cavity could be heated or cooled by circulating a working fluid from a constant temperature bath through multiple channels milled inside the copper bottom plate. To insure good thermal contact between the conducting walls made of aluminum (6061T6) and the bottom plate, a thermal compound was applied to the ends of the aluminum plates. The Plexiglass windows were used to allow for flow visualization, photographic, and shadowgraphic observations. For interferometric measurements, optical quality glass windows were used.

The heated surface temperature of the enclosure including the bottom plate and the two conducting sidewalls was measured by T-type thermocouples which were embedded along the inner surface of the cavity. Numerous thermocouples were also located inside the test cell for measuring the temperatures of the solid and the liquid of the phase-change material.

Test procedure and data reduction

Research grade (99% pure) n-octadecane was used as the material in the experiments. This paraffin was desirable because its fusion temperature is near the ambient

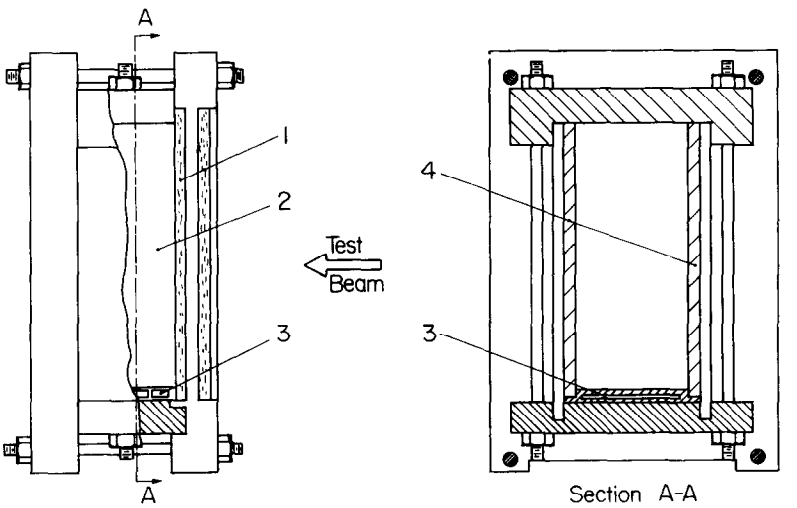

FIG. 1. Schematic diagram of the test cell: (1) Plexiglas window; (2) test region; (3) channels for temperature controlled fluid flow; (4) aluminum conducting walls.

laboratory temperature which aids in reducing heat losses (or gains) to the ambient environment. It is transparent (in the liquid phase) to the visible radiation, and this allows for the photographic observations and optical measurements. In addition, the thermophysical properties of n-octadecane are reasonably well established.

The preparation for a test run always began with the degasification of the phase-change material. The material was contained in a flask having a small side-opening and was heated well above its fusion temperature. Then, by connecting the side-opening of the flask to a vacuum pump the liquid was evacuated for about 3–4 h. During this time the material was allowed to solidify by cooling to the ambient environment and was remelted afterwards. The degasified liquid was carefully syphoned into the test cell. The ambient air temperature was always controlled such that only a small temperature difference existed between the ambient and the fusion temperature of the material.

For the melting experiments, once the test cell was filled with the liquid, the shadowgraph system was aligned. A plastic foil marker with a grid network of the exact contour of the test cell was attached to the screen to identify the orientation of the heat source. Then, the liquid paraffin in the test cell was solidified by circulating cold (below the fusion temperature) working fluid through the channels milled inside the heat source. In the solidification process the upper surface of the unfrozen material appeared to be concave as a result of the volumetric contraction associated with solidification. In order to obtain a flat upper surface of the solid, additional liquid was syphoned into the test cell. After the solidification was completed the temperature of the circulating fluid was adjusted to a preselected value and maintained thereafter so as to establish an initial temperature condition in the solid for the melting experiments that followed. A uniform initial temperature of the solid in the test cell was insured by circulating a coolant for a period of about 8 h. After all of these initial preparations, the melting experiment was started by switching on the second constant temperature bath circulating a hot (above the fusion temperature) working fluid through the base plate.

During the solidification experiments, the initial liquid temperature of the PCM was established by a similar procedure to that in the melting experiments. After the initial liquid temperature had been established, the solidification experiment was started by switching on the second constant temperature bath circulating a cold fluid (below the fusion temperature) through the base plate.

In both melting and solidification experiments, the temperatures were recorded at the preselected time intervals. The solid–liquid interface profiles as well as the images of shadowgraph and the interference fringe patterns during the melting were photographed with a 35 mm Nikon FE camera on Kodak Tri-X film (ASA 400).

The local heat transfer coefficient at the walls of the cavity were measured using a shadowgraph system. The experimental setup employed was identical to that described elsewhere [8], thereby obviating the need for detailed exposition. Experimentally, the shadowgraph technique for heat transfer measurements involves identification of the heat source surface as a reference position as well as the recording of the deflection of the light beam on the screen after its passage through the test cell. To make the deflection of the light beam, which passes through the thin region adjacent to the heat source surface, more visible against the dark background, a plate with a narrow aperture was placed between the collimating lens and the test cell. This aperture blocked off the light entering the test cell except that which passed through the immediate vicinity of the heat source surface.

In both melting and solidification experiments the solid–liquid interface position was photographed at predetermined time intervals. The solid–liquid interface contours were then traced from the photographs. The area of the unmelted solid or unfrozen liquid was evaluated with a planimeter. The accuracy of this device was estimated to be about $\pm 5\%$ for an area of 1 in.^{2} (or 6.45 cm^2).

RESULTS AND DISCUSSION

Melting experiments

Melting patterns. A comprehensive history of the melting process can be obtained by recording photographically the contours of the solid–liquid interface at different times during an experiment. A typical history of the solid–liquid interface motion is presented in Fig. 2 where the solid–liquid interface contours are shown at different instants of time for various aspect ratio enclosures.

At early times, conduction is the only mechanism of heat transfer, as evidenced by the uniform melt thickness along the bottom. A uniform melt layer is seen to recede from the bottom along the vertical sidewalls, except for the region close to the free surface. In this region, melting is significantly faster as a consequence of the density difference between the solid and the liquid which forces the liquid to seek extra space by expanding and thus overflowing the top of the unmelted solid core. The presence of this density-induced melt motion contributes significantly to the early departure of the melting behavior from that of pure conduction.

As time passes, the thermal instability induced in the melt zone directly below the solid core takes place as evidenced by the appearance of the wavy shape of the solid–liquid interface. This irregular shape of the melting front arises from the presence of the unsteady vortex circulation (Bénard convection) in the melt region which produced a hemisphere-capped interface. For small Rayleigh numbers (i.e. melt layer thicknesses) the interface was very regular, but as the Rayleigh number increased the convection cells merged and the

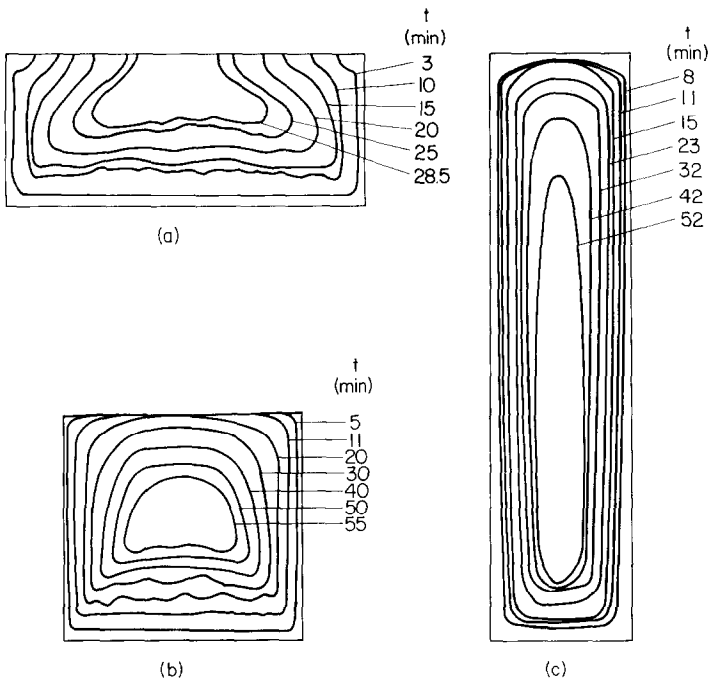

FIG. 2. Solid–liquid interface contours during melting of n-octadecane in a rectangular cavity with conducting walls: (a) $Ste_l = 0.132$, $S_c = 0.004$, $AR = 0.42$; (b) $Ste_l = 0.132$, $S_c = 0.026$, $AR = 1.0$; and (c) $Ste_l = 0.068$, $S_c = 0.096$, $AR = 4.0$.

interface became irregular. The history of the vortex motion in this region was found to be similar to that described elsewhere [15]. As for the region along the vertical walls, the melt layer thickness increases from the bottom edge toward the top. Melting occurs faster at the top, then decreases downward to the bottom and is similar in trend to that observed during melting in an isothermal vertical wall cavity [15]. The density-induced motion and the subsequent establishment of buoyancy-driven convection are responsible for the reversal in the trend of the melt thickness. The melting patterns thereafter are quite similar to those of cavities with isothermal walls. It should be noted that the temperature difference across the walls continued to decrease as the melting progressed [16]. Particularly, for the case of a small aspect ratio ($AR = 0.42$), the conducting walls were acting like isothermal walls due to the small temperature difference along them.

Figure 3 shows the timewise variation of the molten fraction for three different Stefan numbers. The data correlate well by adopting the dimensionless time $\tau_l = Ste_l Fo_l$ as the independent variable. An empirical correlation of best least squares fit has been obtained as

$$V/V_0 = 16.8\tau_l^{0.728}. \quad (1)$$

The effect of the initial subcooling of the solid on the melting process was studied by performing several experiments with different initial temperatures of the solid below its fusion temperature. This is indicated by the magnitude of the subcooling parameter S_c. Figure 4

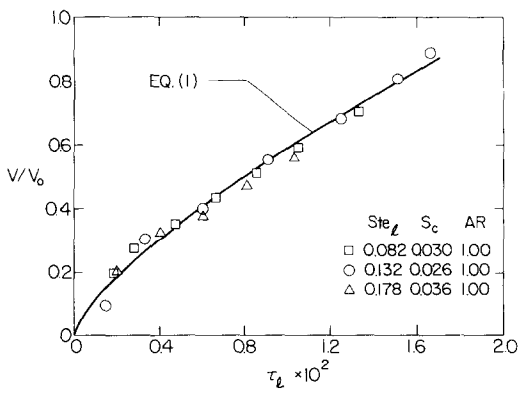

FIG. 3. Correlation for experimental results of the melted volume.

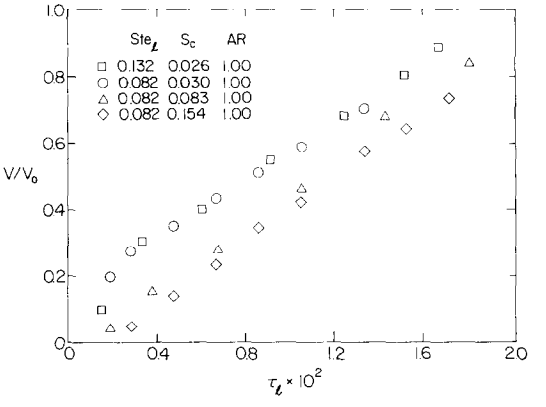

FIG. 4. Effect of initial subcooling on the melting rate in a rectangular cavity with conducting walls, $AR = 1.0$.

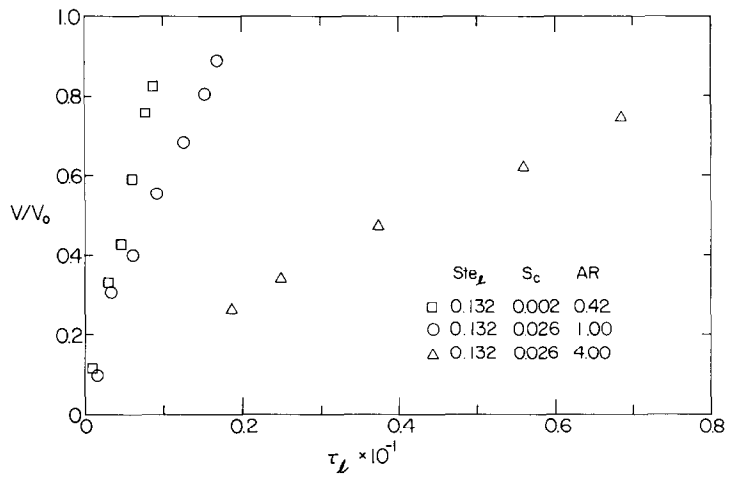

FIG. 5. Effect of aspect ratio of the rectangular cavity on the melting rate.

shows the timewise variation of the molten volume fraction for various subcooling parameters. In order to eliminate the effect of the aspect ratio as a parameter, these experiments were conducted in a cavity having an aspect ratio of unity. It is evident from the figure that the initial subcooling could substantially slow down the melting process, particularly at the early times. This behavior is attributed to the fact that with an initially subcooled solid, only a fraction of the energy transported to the solid–liquid interface is used to melt the solid; the remaining fraction of the energy is used to raise the temperature of the solid core to its fusion temperature. As a result, the progression of the melt region is retarded. The results also show that the onset and development of the buoyancy-driven convection in the melt is delayed because of the relatively thin melt layer in the presence of subcooling. The degree of retardation, however, did not exhibit a linear relationship with the magnitude of the initial subcooling as evidenced by the data shown in Fig. 4 for $S_c = 0.083$ and 0.154, respectively.

Figure 5 presents the timewise variation of the molten fraction for three different aspect ratio enclosures. The effect of the aspect ratio in the range examined indicates that the melting rate decreases sharply as the aspect ratio of the cavity increases. This can be attributed to the fact that in the presence of well-developed natural convection, heat transfer to the melt primarily takes place near the bottom of the vertical walls, and so adding more height to the cavity does little to increase the total heat transfer from the heated surface to the melt; however, the total volume of the material to be melted is increased significantly and as a result the melting rate decreases with the increase in the aspect ratio of the cavity. Attempts to correlate the results and to obtain a general empirical equation for the melt volume fraction were unsuccessful.

Heat transfer. To gain better insight into the unsteady temperature distribution and to infer the convective flow patterns in the liquid during melting, a Mach–Zehnder interferometer having 25 cm diameter optics of typical rectangular design was employed. The interferometer is a desirable instrument for determining a 2-D temperature distribution in steady or unsteady transport processes because it can yield instantaneous information on the 2-D temperature field without disturbing or distorting the flow and temperature fields. However, due to the high sensitivity of the index of refraction of n-octadecane to temperature, it was very difficult to use the interferometer for quantitative heat transfer measurements. In the presence of only a few degrees temperature difference imposed between the heated surface and the solid–liquid interface, the fringe density was too high for accurate location and interpretation of the interferograms, particularly in the vicinity of both the heated surface and the solid–liquid interface. These are the regions of main interest in the study. Thus, the interferograms obtained could only be used for qualitative interpretation of the temperature field and of the convective recirculation patterns in the melt.

Figure 6 shows two photographs of the interference fringe patterns at different times during the course of the melting experiments. The dashed lines in these photographs indicate the contour of the heated surface of the cavity. A single fringe shift represents a temperature difference of approximately 0.0527°C. It can be seen from the photographs that the fringes along the heated surface of the enclosure and the solid–liquid interface appear to be hazy and indistinctive as a result of large fringe density in these regions [Fig. 6(a)]. The timewise variation of the fringe patterns in the region along the conducting walls of the enclosure exhibits a similar trend as that of melting from an isothermal wall cavity [16]. The convection circulation patterns in this region can be inferred from the fringe patterns. The liquid rises along the vertical wall until it reaches the free surface where it takes a 90° turn. The melt then descends along the solid–liquid interface. As time passes, natural convection circulation intensifies. This is evidenced by the presence of the more pronounced

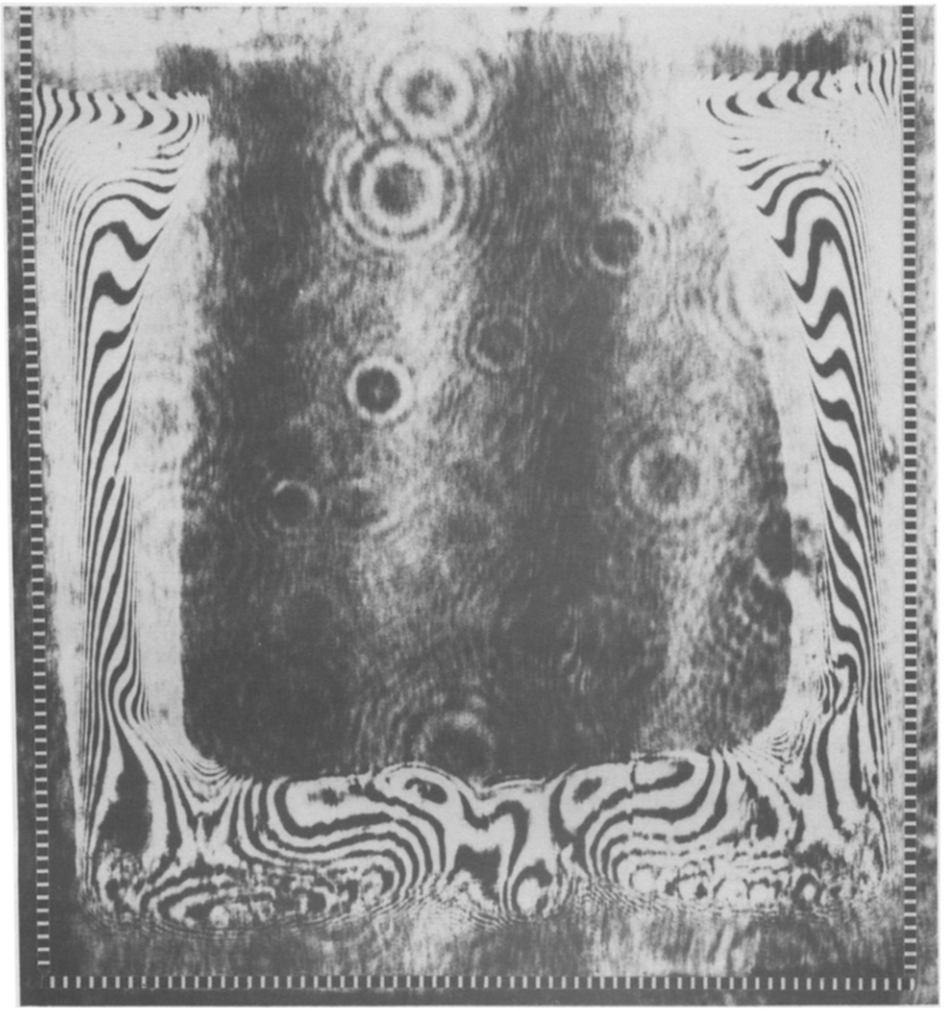

Fig. 6(a).

deflection of the interference fringe lines [Fig. 6(b)]. Another feature worthy of note is the decrease of fringe density with time as a result of the continuous change in the shape and size of the melt region [compare Figs. 6(a) and (b)].

As for the interference fringes along the heated bottom surface of the cavity shown in the photographs, the variation of the fringe patterns with time and position indicates rather complex trends because of the presence of the time-dependent vortex circulation in the region as discussed previously. The timewise variation of 'cellular' flow patterns occurring above the bottom can be confirmed by examination of the timewise variation of the fringe patterns in the region. As the melting continues and the thickness of the melt zone increases, the cellular flow in the bottom melt layer begins to interact with the recirculating flow along the vertical walls. Furthermore, the intensification of recirculation along the sidewalls tends to suppress the cellular flow patterns as the melting progresses [compare Figs. 6(a) and (d)].

Local heat transfer results along the conducting walls determined experimentally by the shadowgraph method are presented in terms of the parameter $Nu_y/Ra_y^{1/4}$ vs the vertical position y/H. The vertical position y was chosen as the characteristic length for both the local Nusselt number Nu_y and the local Rayleigh number Ra_y. It is recognized that the distance y may not be an appropriate length scale for the problem, because the size and shape of the melt region changes with time. Figures 7 and 8 show some typical results of the local heat transfer coefficient variation with time along the conducting walls. Additional results are given elsewhere [16]. Due to the overlap of the shadowgraph images in the corner of the cavity and the free surface, the local heat transfer results in these regions could not be determined. In general, it can be seen that the peak value of the parameter $Nu_y/Ra_y^{1/4}$ decreases as the melting progresses. This indicates transition from the heat conduction mode to the onset of the natural convection dominated melting as the heating continues. Initially, while heat conduction is the dominant heat transfer mechanism, the presence of the melt motion induced by the volume increase associated with the phase change of the material causes a drastic drop in the local heat transfer in the vicinity of

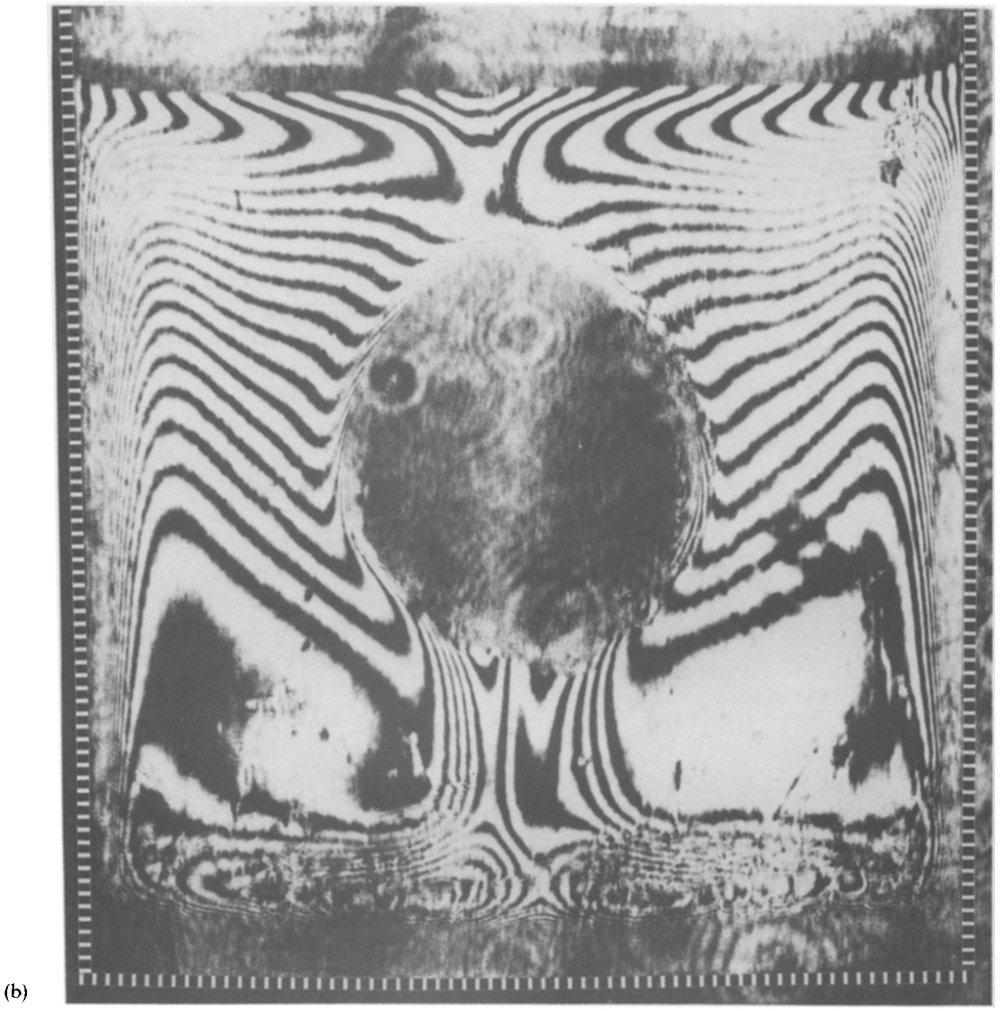

FIG. 6. Photographs of interference fringe images in the liquid n-octadecane during melting in a rectangular cavity with conducting walls, $T_w = 30.4°C$, $AR = 1.0$: (a) $t = 240$ min; and (b) $t = 428$ min.

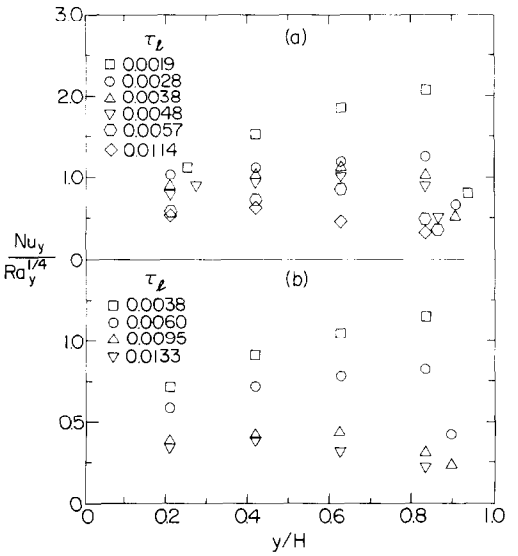

FIG. 7. Variation of the local heat transfer coefficients along the conducting wall during melting: (a) $Ste_l = 0.082$, $S_c = 0.030$, $AR = 1.0$; and (b) $Ste_l = 0.082$, $S_c = 0.154$, $AR = 1.0$.

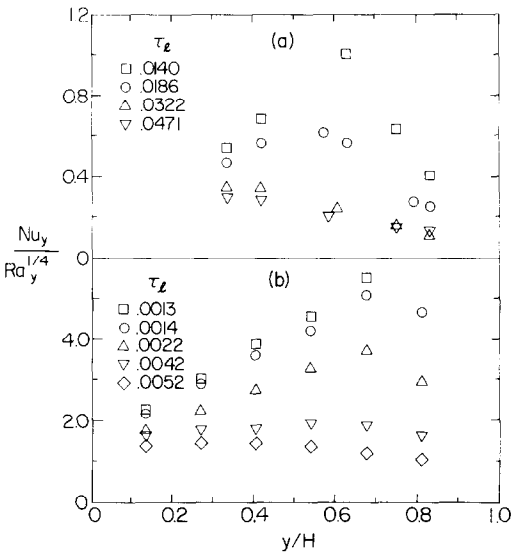

FIG. 8. Variation of the local heat transfer coefficients along the conducting wall during melting: (a) $Ste_l = 0.068$, $S_c = 0.109$, $AR = 0.42$; and (b) $Ste_l = 0.068$, $S_c = 0.096$, $AR = 4.0$.

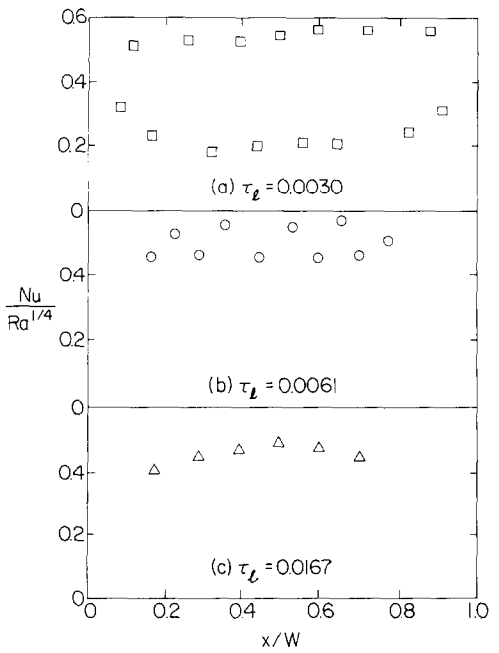

FIG. 9. Variation of the local heat transfer coefficients along the isothermal base surface of the cavity, $Ste_l = 0.132$, $S_c = 0.026$, $AR = 1.0$.

the free surface. As time passes and the temperature difference along the conducting walls continues to decrease, natural convection develops in the melt. The flow is upward along the walls and downward adjacent to the solid–liquid interface. As the melt is carried upward it gains heat and the temperature gradients decrease. The local heat transfer coefficients continue to decrease until nearly quasi-steady values are reached with time. Comparison of the data shown in Fig. 7 reveals that the presence of subcooling has a significant impact on the heat transfer coefficient. This is attributed primarily to heat conduction from the solid–liquid interface toward the solid core. Conduction raises the solid temperature and causes a slowdown of the progression of the interface and delays the onset and development of buoyancy-driven recirculation in the melt. Results of Fig. 8 show that the heat transfer parameter $Nu_y/Ra_y^{1/4}$ increases with an increase in the aspect ratio of the cavity.

Figure 9 shows some typical results for the timewise variation of the local heat transfer coefficients along the heated isothermal bottom surface of the cavity. The width of the base wall of the cavity W was chosen as the characteristic length for both the Nusselt number Nu and the Rayleigh number Ra. A similar history of the time-dependent vortex circulation patterns as this was observed in the melt zone above the base of an isothermal wall cavity [15]. As the melting progresses and natural convection develops, the local Nusselt number exhibits nearly periodic variation with location along the bottom [Figs. 9(a) and (b)]. This is a clear indication of the development of multiple vortex circulation patterns in the melt region. With continued melting, the periodic trend in the Nusselt number distribution tends to abate as evidenced by the decrease in the number of the peaks and the magnitude of the oscillations [Fig. 9(b)]. This is due to the decrease in the number of the vortex cells as the melt zone becomes larger with time. As shown in Fig. 9(c) at late time ($\tau_l = 0.0167$), the local Nusselt number along the bottom surface is almost constant, which indicates that convection is controlled by the major recirculation motion in the liquid at this stage of melting. The aspect ratio of the cavity, the Stefan number and the subcooling parameter all influence heat transfer and its timewise variation at the bottom.

Due to the overlap of the shadowgraphs in the corner regions of the cavity, the local temperature gradients and thus the heat transfer coefficients in these regions could not be determined from the shadowgraph observations. As a result, the determination of the average heat transfer coefficients from the ordinary spatial averaging method appears to be inappropriate. Therefore, as an alternative the energy balance method [8] based on the molten volume fraction, data was employed to determine the average heat transfer coefficients from the heated surface of the cavity. The instantaneous surface-averaged Nusselt number can be expressed as

$$\overline{Nu} = \bar{h} l_{eq}/k_l = 2\left[\frac{AR}{AR+1}\right]^2 \times (V/V_0)^2[1+\tfrac{1}{2}(Ste_l - S_c)]/\tau_l. \quad (2)$$

The characteristic length l_{eq}, based on the instantaneous melt layer thickness, equivalent to a corresponding unidirectional melting problem, is defined as

$$l_{eq} = V/A_h = [H/(2AR+1)](V/V_0). \quad (3)$$

The temperature of the bottom is used to define both the instantaneous Nusselt and the Rayleigh numbers. The data for various Stefan numbers, aspect ratios, and initial subcooling parameters are plotted in Fig. 10. An empirical correlation based on the least squares fit has

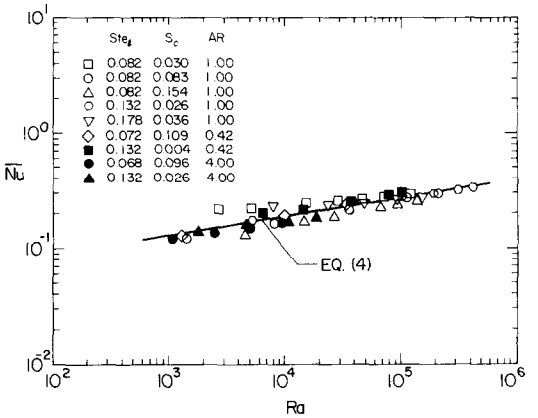

FIG. 10. Average Nusselt number dependence on the average Rayleigh number.

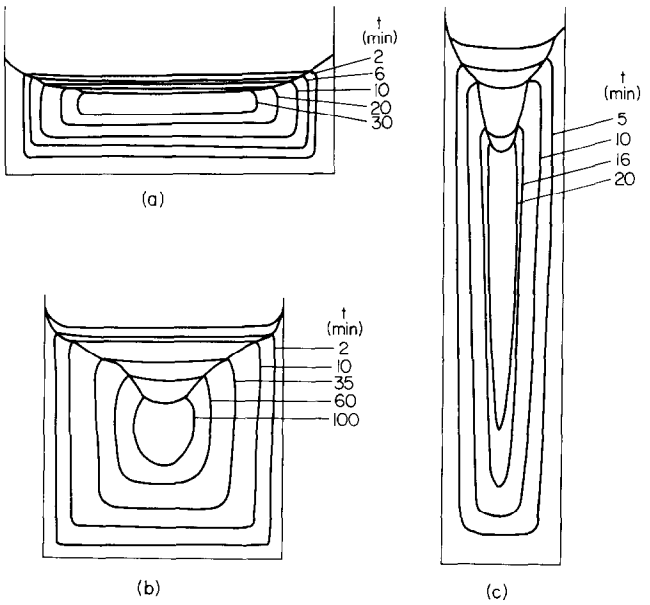

FIG. 11. Solid–liquid interface contours during solidification of n-octadecane in a rectangular cavity with conducting walls: (a) $Ste_s = 0.108$, $S_h = 0.067$, $AR = 0.42$; (b) $Ste_s = 0.109$, $S_h = 0.005$, $AR = 1.0$; and (c) $Ste_s = 0.109$, $S_h = 0.067$, $AR = 4.0$.

been obtained and is of the form

$$\overline{Nu} = 0.189\overline{Ra}^{0.319}. \quad (4)$$

This equation is also plotted as a solid line in the figure. The correlation is for the Rayleigh number range $10^3 \leqslant \overline{Ra} \leqslant 4.1 \times 10^5$.

Solidification experiments

Freezing patterns. Shortly after the cooling was initiated, a thin frost layer of solid was formed on the bottom surface of the cavity. A few seconds later, the solidification along the vertical conducting walls was observed to occur at the bottom edge of the sidewalls propagating upward along the walls. The thickness of the frozen layer increased rather rapidly at early times. Figure 11 depicts the timewise progression of the solid–liquid interface for various Stefan numbers, aspect ratios, and initial superheating parameters. Due to the volume decrease associated with the phase change from the liquid to the solid, the liquid level drops as the solidification proceeds. Consequently, a sloped concave shape of the frozen solid was formed at the free surface as shown in the figures.

Inspection of Fig. 11 reveals that for an aspect ratio of 0.42, the thickness of the frozen layer along the vertical conducting walls is practically uniform. This can be attributed to the small temperature drop along the walls, which resulted not only from the high thermal conductivity of the aluminum but also from the small height of the walls. The height is believed to be the dominant controlling factor. Based on the above observation, it should be expected that the higher the aspect ratio the greater is the slope of the frozen layer along the conducting walls. This statement can be verified by examining Figs. 11(b) and (c) for aspect ratios of 1.0 and 4.0, respectively.

Frozen volume fraction. The effect of the Stefan number during solidification can be analyzed by presenting the data as a function of the dimensionless time $\tau_s (= Ste_s Fo_s)$ as is done in Fig. 12. All of the experimental data collapse quite nicely onto a single curve. A correlation based on the best least squares fit has also been obtained in the form

$$V/V_0 = 1.02 \text{ erf } (5.95\tau_s^{1/2}), \quad (5)$$

and is plotted as the solid line in the figure. As for the independent influence of the initial superheating of the liquid on the solidification process, the results showed that the initial superheating of the liquid dissipated rapidly and the influence of the superheating could only be observed at early times of the solidification process. The results presented in Fig. 12 further illustrate this

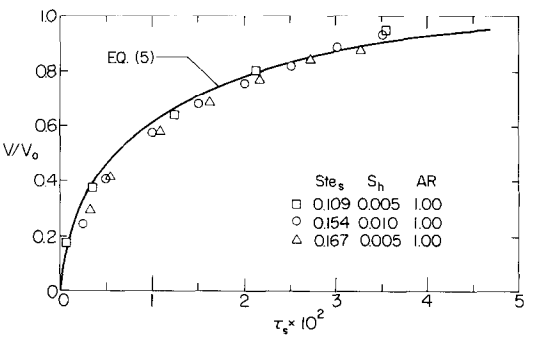

FIG. 12. Correlation for the experimental results of the frozen volume.

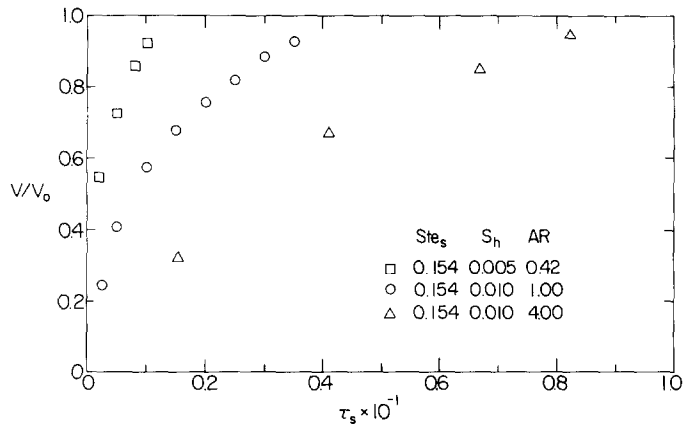

FIG. 13. Effect of aspect ratio of the cavity on the freezing rate in a rectangular cavity with conducting vertical walls.

point. The Stefan numbers as well as the aspect ratio of the cavity for these experiments were maintained nearly the same.

A numerical solution of freezing in a rectangular enclosure with vertical conducting walls has been reported [12]. However, since the dimensionless parameters covered in the present study are quite different from those of their numerical study, the experimental data obtained in this work cannot be compared directly with the predictions. Qualitatively, the experimental findings of the enhancement of solidification rate for a small aspect ratio cavity, as shown in Fig. 13, was also predicted in the analysis. The results of the figure clearly show that long fins (conducting walls) are not effective in increasing heat transfer during solidification.

CONCLUSIONS

The experimental results have clearly established that the melting rate, the melt front profiles, and the heat transfer are significantly affected by the fluid motion in the melt induced by the buoyancy force (natural convection) and by volumetric expansion accompanying the phase change from the solid to the liquid. The latter are particularly significant at the early times while the heat transfer is still dominated by conduction. The initial subcooling of the solid significantly impedes the melting process, because a portion of the energy transported to the solid–liquid interface is absorbed as sensible heat by the solid and as a result the melting process slows down. This slowdown of melting also causes a delay in the onset and development of the buoyancy-driven recirculation in the melt.

The formation of the boundary layers adjacent to the solid–liquid interface and along the heated surfaces has been inferred from the interference fringe patterns in the liquid during the melting in a rectangular cavity with conducting vertical walls. A vortex cellular motion similar to that which occurred in a rectangular cavity with isothermal walls was observed to occur at the melt region above the isothermal base surface.

During solidification the initial superheating of the liquid in rectangular cavities dissipated rather quickly so that the significance of this effect on the solidification could be seen only early in the process. As the aspect ratio of the rectangular cavity increased, the solidification rate decreased. Short extended surfaces are more effective than longer ones.

Acknowledgements—The work described in the paper was supported by the National Science Foundation Heat Transfer Program through Grant MEA-8014061.

REFERENCES

1. R. Viskanta, Phase-change heat transfer, in *Solar Heat Storage: Latent Heat Materials* (edited by G. A. Lane), Chap. 5. CRC Press, Boca Raton, Florida (1983).
2. H. S. Carslaw and J. C. Jaeger, *Conduction of Heat in Solids* (2nd edn.). Clarendon Press, Oxford (1959).
3. R. Viskanta, J. C. Mollendorf and K. T. Yang, Melting and solidification, in *Proceedings of the Natural Convection Workshop* (edited by K. T. Yang and J. R. Lloyd), Breckenridge, Colorado, 18–21 July 1982, University of Notre Dame, Notre Dame, Indiana (1982).
4. W. R. Humphries, Performance of finned thermal capacitors, NASA TN D-7890, Washington, DC (1974).
5. W. R. Humphries and E. I. Griggs, A design handbook for phase change thermal control and energy storage devices, Technical Paper 1074, NASA, Washington, DC (1977).
6. A. Abhat, S. Aboul-Enein und G. Neuer, Latenwarmespeicher zur Vervendung in Solar-Energie-Systemen fur Wohngebaude, *VDI-Ber.* No. 288, 97–104 (1977).
7. A. Abhat, G. Dietrich and H. Hage, Study and design of a modular phase change material capacitor for application to spacelab payloads, AIAA Paper No. 78-887 (1978).
8. A. G. Bathelt and R. Viskanta, Heat transfer and interface motion during melting and solidification around a finned horizontal sink/source, *J. Heat Transfer* **103**, 720–726 (1981).
9. E. M. Sparrow, E. D. Larson and J. W. Ramsey, Freezing on a finned tube for either conduction-controlled or natural convection-controlled heat transfer, *Int. J. Heat Mass Transfer* **24**, 273–284 (1981).

10. F. P. Griffin and R. N. Smith, Approximate solutions for freezing adjacent to an extended surface, ASME Paper No. 80-HT-8 (1980).
11. R. H. Heinze and J. A. C. Humphrey, Enhanced heat conduction in phase-change thermal energy storage devices, *Int. J. Heat Mass Transfer* **24**, 459–474 (1981).
12. R. N. Smith and J. Koch, Numerical solution for freezing adjacent to a finned surface, in *Heat Transfer—1982* (edited by U. Grigull *et al.*), Vol. 2, pp. 67–74. Hemisphere, Washington, DC (1982).
13. B. Yimer, J. N. Crisp and E. T. Mahefkey, Transient thermal analysis of phase change thermal energy storage systems, ASME Paper No. 80-HT-2 (1980).
14. J. W. Sheffield, Effects of doubly-connected finned surfaces on heat transfer during solidification, AIAA Paper No. 82-0847 (1982).
15. C. J. Ho and R. Viskanta, Experimental study of melting in a rectangular cavity, in *Heat Transfer—1982* (edited by U. Grigull *et al.*), Vol. 2, pp. 369–374. Hemisphere, Washington, DC (1982).
16. C. J. Ho, Solid–liquid phase change heat transfer in enclosures, Ph.D. thesis, Purdue University, West Lafayette, Indiana (1982).

TRANSFERT THERMIQUE DE CHANGEMENT DE PHASE SOLIDE–LIQUIDE INTERNE A UNE CAVITE RECTANGULAIRE AVEC DES PAROIS VERTICALES CONDUCTRICES

Résumé—On traite des transferts thermiques à l'interface solide–liquide pendant le changement de phase (fusion ou solidification) du n-octadécane dans une cavité rectangulaire bidimensionnelle avec des parois verticales conductrices. La technique des ombres est utilisée pour mesurer les coefficients locaux de transfert thermique à la surface de la source de chaleur. Le mouvement de l'interface solide–liquide pendant le changement de phase est photographié. Pendant la fusion, on observe le développement d'un tourbillon au bas de la zone de fusion qui ressemble à celui dans une cavité rectangulaire avec parois isothermes. Dans les expériences de fusion et de solidification les parois conductrices agissent comme des surfaces isothermes pendant les derniers instants des mécanismes. La convection naturelle contrôle la forme de la zone fondue, la vitesse de fusion et le transfert thermique pendant la fusion. L'effect du non-refroidissement initial du solide est aussi étudié et les résultats montrent clairement que la conduction thermique est le mode dominant de transport d'énergie pendant la solidification. Pour le transfert thermique de changement de phase solide–liquide, des surfaces excroissantes courtes sont plus efficaces que les longues.

NACH INNEN GERICHTETER WÄRMETRANSPORT BEIM FEST/FLÜSSIG-PHASENWECHSEL IN EINEM RECHTECKIGEN HOHLRAUM MIT LEITENDEN VERTIKALEN WÄNDEN

Zusammenfassung—Der Bericht behandelt grundlegende Gegebenheiten der Fest/Flüssig-Grenzfläche und des Wärmetransports, die während des Fest/Flüssig-Phasenwechsels (Schmelzen und Erstarrung) von n-Oktadekan in einem zweidimensionalen rechteckigen Hohlraum mit leitenden senkrechten Wänden ermittelt wurden. Mit Hilfe des Schattenschlierenverfahrens wurden die örtlichen Wärmeübergangskoeffizienten an der Oberfläche der Heizfläche gemessen. Die Wanderung der Fest/Flüssig-Grenzfläche während des Phasenwechsels wurde fotografisch aufgezeichnet. Während des Schmelzens wurde an der unteren Schmelzzone eine Wirbelbildung beobachtet, welche derjenigen in einem rechteckigen Hohlraum mit isothermen Wänden ganz ähnlich ist. Bei sowohl Schmelz- als auch Erstarrungsversuchen verhielten sich die leitenden Wände am Ende der Vorgänge wie isotherme Wände. Es zeigte sich, daß die freie Konvektion die Form der Schmelzfront, die Schmelzgeschwindigkeit und den Wärmeübergang bestimmt. Der Einfluß anfänglicher Unterkühlung der festen Phase wurde ebenfalls untersucht, und die Ergebnisse zeigten klar, daß die Wärmeleitung den Hauptmechanismus des Energietransports während der nach innen fortschreitenden Erstarrung darstellt. Beim Fest/Flüssig-Phasenwechsel sind hinsichtlich des Wärmetransport kürzere Rippen effektiver als längere.

ТЕПЛОПЕРЕНОС ПРИ НАПРАВЛЕННОМ ВНУТРЬ ФАЗОВОМ ПЕРЕХОДЕ (ПЛАВЛЕНИИ И ЗАТВЕРДЕВАНИИ) В ПРЯМОУГОЛЬНОЙ ПОЛОСТИ С ТЕПЛОПРОВОДЯЩИМИ ВЕРТИКАЛЬНЫМИ СТЕНКАМИ

Аннотация—Представлены основные результаты исследования границы раздела твердое тело—жидкость и теплопереноса при фазовом переходе (плавлении и затвердевании) н-октадекана в двумерной прямоугольной полости с теплопроводящими вертикальными стенками. Измерения коэффициентов локального теплопереноса на поверхности нагрева проводились методом теневой фотографии. Перемещение границы раздела между твердым телом и жидкостью при фазовом переходе регистрировалось фотографически. Показано, что при плавлении вихревые движения в нижней зоне плавления развиваются совершенно аналогично случаю с изотермическими стенками. В экспериментах как по плавлению, так и затавердеванию теплопроводящие стенки вели себя в конечные периоды времени развития процессов как изотермические. Показано, что естественная конвекция определяет форму расплава, скорость плавления и теплоперенос при плавлении. Исследовалось также влияние начального недогрева твердого тела. Результаты показали, что при направленном внутрь затвердевании энергия переносится главным образом теплопроводностью. Для интенсификации теплопереноса при фазовом переходе короткие развитые поверхности более эффективны, чем длинные.